

Phase Distribution Control of a Population of Oscillators

Bharat Monga* and Jeff Moehlis†

Abstract. The collective behavior of biological oscillators has been recognized as an important problem for several decades, but its control has come into limelight only recently. Much of the focus for control has been on desynchronization of an oscillator population, motivated by the pathological neural synchrony present in essential and parkinsonian tremor. Other applications, such as the beating of the heart and insulin secretion, require synchronization, and recently there has been interest in forming clusters within an oscillator population as well. In this article, we devise a unified control framework to achieve all of these distinct collective behaviors observed in biological oscillators. The control algorithm is based on the partial differential equation governing the evolution of the phase distribution of a population of identical, uncoupled oscillators. Motivated by pathological neural synchrony, we apply our control to desynchronize an initially synchronized neural population. Given the proposed importance of enhancing spike time dependent plasticity to stabilize neural clusters and counteract pathological neural synchronization, we formulate the phase difference distribution in terms of the phase distribution, and prove some of its fundamental properties, and in turn apply our control to transform the neural phase distribution to form clusters. Finally, motivated by eliminating cardiac alternans, we apply our control to phase shift a synchronous cardiac pacemaker cell population. For the systems considered in this paper, the control algorithms can be applied to achieve any desired traveling-wave phase distribution, as long as the combination of the initial phase distribution and phase response curve is non-degenerate. To demonstrate the effectiveness of our control for each of these applications, we show that a population of 100 phase oscillators with the applied control mimics the desired phase distribution.

Key words. Biological systems; Distributed parameter systems; Pseudospectral methods; Phase Reduction

1. Introduction. Populations of nonlinear oscillators are found in a variety of applications from physics, chemistry, biology, and engineering [49, 30, 66, 25]. The collective behavior of such oscillators varies, and includes synchronization, desynchronization, and clustering. For example, synchronization in beta cells is crucial for efficient insulin secretion [54], the beating of the heart is regulated by constant pacing of synchronized cardiac pacemaker cells [35, 48], and neural synchrony is essential in visual and odor processing [17, 15], and also in learning and memory recall [56, 27]. However, synchronization can be detrimental as well. For example, pathological neural synchronization in the thalamus and the subthalamic nucleus (STN) brain region is hypothesized to be one of the causes of motor symptoms for essential and parkinsonian tremor, respectively [24, 28]; this motivates the goal of designing a control input to desynchronize an oscillator population. Recently there has also been focus on achieving partial synchrony through clustering instead of complete neural desynchronization [33, 34, 63]. One motivation behind such clustering is to rewire neural connections by enhancing spike time dependent plasticity which potentiates intra-cluster synaptic connections and depresses inter-cluster connections. This potentially helps in long-term stabilizability of the clusters in the

*Mechanical Engineering Department University of California at Santa Barbara, Santa Barbara, CA 93106 (monga@ucsb.edu).

†Mechanical Engineering Department University of California at Santa Barbara, Santa Barbara, CA 93106 (moehlis@engineering.ucsb.edu).

Under Review since July 7 2018

presence of noise.

Such diversity of collective behavior has motivated researchers to develop specific control techniques to achieve different behaviors. For example, [69, 13, 31] develop control to promote synchrony, [59, 61, 62] develop control to promote desynchronization, and [33, 34] develops ways to promote clustering. We note that some of these previously proposed algorithms to promote collective behavior are based on individual neuron models [40, 11, 45, 62], and some can face implementation challenges if they require observability of phases of all neurons at all times [45], or demand initial phases to be sufficiently close [62, 60]. There are also population-level algorithms for desynchronization in the literature which use multiple inputs [58, 59, 60], making experimental implementation challenging because they require multiple electrodes to be implanted in a small region of brain tissue.

In this article we overcome these difficulties by developing a unified control framework based on a population-level model which can achieve all of the collective behaviors mentioned above using a single control input. Our algorithm is based on phase reduction, a classical reduction technique based on isochrons [18], which has been instrumental in the development of many of the above control algorithms. It reduces the dimensionality of a dynamical system with a periodic orbit to a single phase variable, and captures the oscillator's phase change due to an external perturbation through the phase response curve (PRC). This can make the analysis of high dimensional systems more tractable, and their control [40, 62, 71, 60, 37, 41] experimentally implementable; see e.g., [57, 46, 55, 71].

The algorithm presented in this paper uses a partial differential equation (PDE) formulation which governs the evolution of the probability distribution of phases (phase distribution) of a population of identical, uncoupled oscillators [8, 60]. We use Fourier analysis to decompose this PDE into a system of ordinary differential equations (ODEs) governing the evolution of the Fourier coefficients of the phase distribution. Thus, to transform the phase distribution of an oscillator population to a desired distribution, we drive the corresponding Fourier coefficients to the Fourier coefficients of the desired distribution. Note that a related control algorithm has been published in [42], where we did not employ Fourier analysis to decompose the PDE into a systems of ODEs, but like the present algorithm it also decreases the L^2 norm difference between the current and the desired phase distributions. For numerical simulation of the control in [42], we used a method of lines type approach, but numerical dissipation present in this approach limited the effectiveness of control, especially when going from a uniform phase distribution to a synchronous distribution. This motivated us to use a pseudospectral method for numerical simulations of our PDEs, to limit numerical dissipation. This further motivated us to re-formulate our control problem in Fourier space as well, which allowed us to arrive at the degenerate set of phase distributions and phase response curves for which the control would not work. Other control algorithms based on the probability distribution of phases include [62, 65].

Motivated by the pathological neural synchronization in the STN and the thalamus as one of the hypothesized causes of motor symptoms of parkinsonian and essential tremor, respectively, we will apply our control algorithm to drive an initially synchronous phase distribution to a uniform distribution. However, total desynchronization may not be desirable, as spike time dependent plasticity in the presence of noise can synchronize an initial desynchronized population [50]. We suggest forming clusters of neurons as an alternative partial desynchro-

nization strategy, and show that the spike time dependent plasticity can help maintain such partial desynchrony by re-wiring synaptic connections between neuron clusters. For this we define a phase difference distribution as a distribution of phase differences between any two oscillators of the population, and prove some of its fundamental properties. We will then use our control algorithm to transform an initially desynchronized neural population into neuron clusters. Motivated by eliminating cardiac alternans, we also use our control algorithm to phase shift a population of synchronized cardiac pacemaker cells. Finally, we devise another similar control algorithm which takes into account the effect of white noise on the oscillator population. To demonstrate the effectiveness of our control for each of these applications, we apply it to a population of 100 uncoupled phase oscillators, and show that the population of phase oscillators with the applied control mimics the desired phase distribution.

This article is organized as follows. In Section 2, we give background on phase reduction, the partial differential equation for the phase distribution, and spike time dependent plasticity. We also formulate the phase difference distribution in terms of the phase distribution and prove some of its fundamental properties. In Section 3, we develop a pseudospectral framework to write distributions as a finite Fourier series, and devise a control algorithm to control their Fourier coefficients. We also construct a degenerate set of phase distributions and phase response curves for which the control would not work. We conclude the section by detailing numerical methods used for generating results for the next section. In Section 4 we demonstrate versatility of our control through several diverse applications and show the corresponding simulation results. In Section 5, we devise a new control to take into account the effect of white noise on the oscillator population. Section 6 summarizes our work and concludes by suggesting future extensions and tools needed for experimental implementation of our algorithm. We note that beyond using a formulation in terms of Fourier series, other improvements and extension with respect to [42] include the discussion of degeneracy, the addition of noise, and novel applications, including the incorporation of the phase difference distribution and plasticity into the control set-up.

2. Background. In this section, we give background on the key concepts of phase reduction, phase response curves, and the partial differential equation for the evolution of the phase density. These will be crucial for the formulation of our control algorithms in Section 3.

2.1. Phase Reduction. Phase reduction is a classical technique to describe the dynamics near a periodic orbit. It works by reducing the dimensionality of a dynamical system to a single phase variable θ [66, 30]. Consider a general n -dimensional dynamical system given by

$$(1) \quad \frac{d\mathbf{x}}{dt} = F(\mathbf{x}), \quad \mathbf{x} \in \mathbb{R}^n, \quad (n \geq 2).$$

Suppose this system has a stable periodic orbit $\gamma(t)$ with period T . For each point \mathbf{x}^* in the basin of attraction of the periodic orbit, there exists a corresponding phase $\theta(\mathbf{x}^*)$ such that

$$(2) \quad \lim_{t \rightarrow \infty} \left| \mathbf{x}(t) - \gamma \left(t + \frac{T}{2\pi} \theta(\mathbf{x}^*) \right) \right| = 0,$$

where $\mathbf{x}(t)$ is the flow of the initial point \mathbf{x}^* under the given vector field. The function $\theta(\mathbf{x})$ is called the *asymptotic phase* of \mathbf{x} , and takes values in $[0, 2\pi)$. For neuroscience applications,

we typically take $\theta = 0$ to correspond to the neuron firing an action potential. *Isochrons* are level sets of this phase function, and it is typical to define isochrons so that the phase of a trajectory advances linearly in time both on and off the periodic orbit, which implies that

$$(3) \quad \frac{d\theta}{dt} = \frac{2\pi}{T} \equiv \omega$$

in the entire basin of attraction of the periodic orbit. Now consider the system

$$(4) \quad \frac{d\mathbf{x}}{dt} = F(\mathbf{x}) + U(t), \quad \mathbf{x} \in \mathbb{R}^n,$$

where $U(t) \in \mathbb{R}^n$ is an infinitesimal control input. Phase reduction can be used to reduce this system to a one-dimensional system given by [67, 29, 8, 43]:

$$(5) \quad \dot{\theta} = \omega + U(t)^T \mathcal{Z}(\theta).$$

Here $\mathcal{Z}(\theta) \equiv \nabla_{\gamma(t)}\theta \in \mathbb{R}^n$ is the gradient of phase variable θ evaluated on the periodic orbit and is referred to as the (*infinitesimal*) *phase response curve (PRC)*. It quantifies the effect of an infinitesimal control input on the phase of a periodic orbit.

In this article we consider control inputs of the form $U(t) = [u(t), 0, \dots, 0]^T$. This comes into phase reduction as $\dot{\theta} = \omega + \mathcal{Z}_1(\theta)u(t)$, where $\mathcal{Z}_1(\theta)$ is the first component of the PRC. Without loss of generality, we will do away with the subscripts and write the first component of PRC as $\mathcal{Z}(\theta)$. Thus the phase reduction is written as

$$(6) \quad \dot{\theta} = \omega + \mathcal{Z}(\theta)u(t).$$

Note that such a control input is motivated by the applications we consider in this article, where only one of the elements of the state vector is affected directly by the control input. The control algorithm in this article can be formulated for a more general control input as well, but as a matter of convenience, we only consider control input of the above form.

2.2. Phase density equation. Given a population of noise-free, identical, uncoupled oscillators all receiving the same control input, it is convenient to represent the population dynamics in terms of its probability distribution $\rho(\theta, t)$, with the interpretation that $\rho(\theta, t)d\theta$ is the probability that a oscillator's phase lies in the interval $[\theta, \theta + d\theta]$ at time t . This evolves according to the advection equation [8, 60, 42]

$$(7) \quad \frac{\partial \rho(\theta, t)}{\partial t} = -\frac{\partial}{\partial \theta} [(\omega + \mathcal{Z}(\theta)u(t)) \rho(\theta, t)].$$

The desired final probability distribution $\rho_f(\theta, t)$ will be taken to be a traveling wave which evolves according to [42]

$$(8) \quad \frac{\partial \rho_f(\theta, t)}{\partial t} = -\omega \frac{\partial \rho_f(\theta, t)}{\partial \theta}.$$

Note that (8) is of the same form as (7) with $u(t) = 0$. Since these are probability distributions, it is necessary that $\int_0^{2\pi} \rho(\theta, t)d\theta = \int_0^{2\pi} \rho_f(\theta, t)d\theta = 1$

In Section 3, we will show how these two equations can be used to devise our control algorithms.

2.3. Phase Difference Distribution. Here we formulate the phase difference distribution in terms of the phase distribution, and prove some of its fundamental properties.

Given a phase distribution $\rho(\theta, t)$ governing the probability of a population of oscillators at phase θ and time t , a corresponding phase difference distribution $\rho_d(\phi, t)$ governs the probability that the phase difference between any two set of oscillators in the population is ϕ at time t , where $\phi \in [0, 2\pi)$. We only consider uncoupled oscillators which evolve independently from each other in this article. Thus the probability that the phase difference between any two oscillators is ϕ at time t can be given by the integral of the products of the phase distribution and the phase distribution shifted by ϕ at times t over the entire domain:

$$(9) \quad \rho_d(\phi, t) = \int_0^{2\pi} \rho(\theta_s, t) \rho(\theta_s + \phi, t) d\theta_s.$$

The phase difference distribution satisfies

$$(10) \quad \int_0^{2\pi} \rho_d(\phi, t) d\phi = 1.$$

This can be show from equation (9):

$$\begin{aligned} \int_0^{2\pi} \rho_d(\phi, t) d\phi &= \int_0^{2\pi} \left[\int_0^{2\pi} \rho(\theta_s, t) \rho(\theta_s + \phi, t) d\theta_s \right] d\phi \\ &= \int_0^{2\pi} \left[\int_0^{2\pi} \rho(\theta_s + \phi, t) d\phi \right] \rho(\theta_s, t) d\theta_s \\ &= \int_0^{2\pi} 1 \cdot \rho(\theta_s, t) d\theta_s \\ &= 1. \end{aligned}$$

Note that phase difference distribution for a time-dependent traveling wave $\rho_f(\theta, t)$ governed by equation (8), is stationary and does not depend on time. This can be proven by taking the time derivative of equation (9):

$$\begin{aligned} \frac{d\rho_d}{dt} &= \int_0^{2\pi} \left[\frac{\partial \rho_f(\theta_s, t)}{\partial t} \rho_f(\theta_s + \phi, t) + \rho_f(\theta_s, t) \frac{\partial \rho_f(\theta_s + \phi, t)}{\partial t} \right] d\theta_s \\ &= -\omega \int_0^{2\pi} \left[\frac{\partial \rho_f(\theta_s, t)}{\partial \theta_s} \rho_f(\theta_s + \phi, t) + \rho_f(\theta_s, t) \frac{\partial \rho_f(\theta_s + \phi, t)}{\partial \theta_s} \right] d\theta_s \\ &= -\omega \rho_f(\theta_s, t) \rho_f(\theta_s + \phi, t) \Big|_0^{2\pi} + \omega \int_0^{2\pi} \rho_f(\theta_s, t) \frac{\partial \rho_f(\theta_s + \phi, t)}{\partial \theta_s} d\theta_s \\ &\quad - \omega \int_0^{2\pi} \rho_f(\theta_s, t) \frac{\partial \rho_f(\theta_s + \phi, t)}{\partial \theta_s} d\theta_s \\ &= 0. \end{aligned}$$

Here, the first equality follows from the Leibniz rule from elementary calculus, and the third equality follows from the previous line by applying integration by parts and imposing periodic

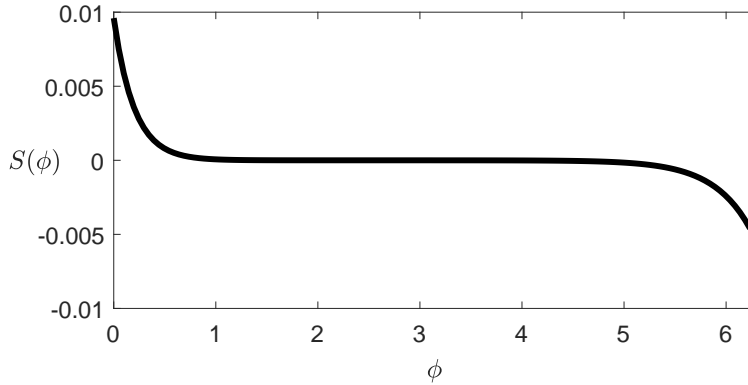


Figure 1. *Spike time dependent plasticity curve: This curve shows the change in synaptic weight between two neurons as a function of their phase difference.*

boundary conditions. Thus, this proves that the phase difference distribution for a time-dependent traveling wave is independent of time. For such a traveling wave phase distribution, we write the phase difference distribution as being independent of time:

$$(11) \quad \rho_d(\phi) = \int_0^{2\pi} \rho_f(\theta_s, t) \rho_f(\theta_s + \phi, t) d\theta_s.$$

2.4. Spike Time Dependent Plasticity. Spike time dependent plasticity (STDP) is an asymmetric form of Hebbian learning [21] that modifies synaptic connections between neurons when they fire repeatedly in a causal manner [6, 7, 32]. At the single synapse level, STDP potentiates (resp., depresses) the synaptic strength for repeated pre-synaptic action potentials arriving just before (resp., after) the post-synaptic action potential. At the population level, STDP strengthens the synaptic connections between neurons that fire action potentials synchronously and weakens those connections in the out of phase neurons [50]. Plasticity is known to be an important factor in the formation of neural pathways in initial brain development, as well as later in learning and memory storage. Since we consider uncoupled oscillating neurons in this article, we reformulate STDP in terms of the phase difference ϕ between two neurons instead of their spike time difference; the distribution of interspike intervals is same as the phase difference distribution for uncoupled oscillating neurons. If the phase difference $\phi \in [0, \pi)$, the STDP would increase the synaptic weight, and if the phase difference $\phi \in [\pi, 2\pi)$, STDP would depress the synaptic weight. We call this increase or decrease of synaptic weights as a function of phase difference the *STDP curve* given as

$$(12) \quad S(\phi) = \begin{cases} pe^{-\frac{\phi}{\tau_p}}, & \phi \in [0, \pi) \\ -de^{\frac{\phi-2\pi}{\tau_d}}, & \phi \in [\pi, 2\pi) \end{cases}.$$

We take the parameters $p = 0.0096$, $d = 0.0053$ from [7], while $\tau_p = 0.2$, $\tau_d = 0.365$ are taken so that the integral of the resulting STDP curve ($\int_0^{2\pi} S(\phi) d\phi$) is zero [70]. Figure 1 shows the STDP curve $S(\phi)$ with the above parameters.

3. Control Algorithm. In this section, we devise a control algorithm to change the probability distribution of a population of oscillators. We do this by approximating the probability distribution as a finite Fourier series and controlling its Fourier coefficients. This algorithm can be applied to a network of noise-free, identical, uncoupled oscillators to achieve any desired traveling-wave probability distribution, as long as the combination of phase distributions and the phase response curve is non-degenerate. A related control algorithm was given in [42], but here we formulate the algorithm in terms of Fourier coefficients; this is better suited for determining the control input using a pseudospectral method which does not have numerical dissipation unlike the method of lines approach used in [42].

3.1. Phase and Phase difference distributions. To devise our control laws, we use the approximation of a finite Fourier series to write the phase distributions and the PRC as

$$(13) \quad \rho(\theta, t) = \frac{1}{2\pi} + \sum_{l=1}^{N-1} [A_l(t) \cos(l\theta) + B_l(t) \sin(l\theta)],$$

$$(14) \quad \rho_f(\theta, t) = \frac{1}{2\pi} + \sum_{l=1}^{N-1} [\widetilde{A}_l(t) \cos(l\theta) + \widetilde{B}_l(t) \sin(l\theta)],$$

$$(15) \quad \mathcal{Z}(\theta) = C_0 + \sum_{l=1}^{N-1} [C_l \cos(l\theta) + S_l \sin(l\theta)].$$

Here N is a large number, so the effect of the omitted higher order Fourier modes is negligible. Writing the distribution this way automatically ensures that the phase distribution is 2π -periodic, and that the total probability $\int_0^{2\pi} \rho(\theta, t) d\theta = 1$ at all times. Multiplying equation (13) by $\cos(k\theta)$ and $\sin(k\theta)$ on both sides and integrating from 0 to 2π with respect to θ , we obtain

$$A_k(t) = \frac{1}{\pi} \int_0^{2\pi} \rho(\theta, t) \cos(k\theta) d\theta,$$

$$B_k(t) = \frac{1}{\pi} \int_0^{2\pi} \rho(\theta, t) \sin(k\theta) d\theta.$$

Taking the derivative with respect to time of the above equations,

$$\dot{A}_k(t) = \frac{1}{\pi} \int_0^{2\pi} \frac{\partial \rho(\theta, t)}{\partial t} \cos(k\theta) d\theta = -\frac{1}{\pi} \int_0^{2\pi} \frac{\partial}{\partial \theta} [(\omega + \mathcal{Z}(\theta)u(t)) \rho(\theta, t)] \cos(k\theta) d\theta,$$

$$\dot{B}_k(t) = \frac{1}{\pi} \int_0^{2\pi} \frac{\partial \rho(\theta, t)}{\partial t} \sin(k\theta) d\theta = -\frac{1}{\pi} \int_0^{2\pi} \frac{\partial}{\partial \theta} [(\omega + \mathcal{Z}(\theta)u(t)) \rho(\theta, t)] \sin(k\theta) d\theta.$$

Integrating these equations by parts and imposing periodic boundary conditions, we obtain

$$(16) \quad \dot{A}_k(t) = -k\omega B_k - \mathcal{I}_{kA}(t)u(t),$$

$$(17) \quad \dot{B}_k(t) = k\omega A_k + \mathcal{I}_{kB}(t)u(t),$$

where

$$(18) \quad \mathcal{I}_{kA}(t) = \frac{k}{\pi} \int_0^{2\pi} \mathcal{Z}(\theta) \rho(\theta, t) \sin(k\theta) d\theta,$$

$$(19) \quad \mathcal{I}_{kB}(t) = \frac{k}{\pi} \int_0^{2\pi} \mathcal{Z}(\theta) \rho(\theta, t) \cos(k\theta) d\theta.$$

Similarly we obtain following equations for time derivatives of \widetilde{A}_k and \widetilde{B}_k :

$$(20) \quad \dot{\widetilde{A}}_k(t) = -k\omega \widetilde{B}_k(t),$$

$$(21) \quad \dot{\widetilde{B}}_k(t) = k\omega \widetilde{A}_k(t).$$

The Fourier coefficients for the phase difference distribution can be calculated as follows:

$$\begin{aligned} \rho_d(\phi) &= \int_0^{2\pi} \left(\frac{1}{2\pi} + \sum_{k=1}^{N-1} \left[\widetilde{A}_k(t) \cos(k\theta_s) + \widetilde{B}_k(t) \sin(k\theta_s) \right] \right) \\ &\quad \times \left(\frac{1}{2\pi} + \sum_{l=1}^{N-1} \left[\widetilde{A}_l(t) \cos(l(\theta_s + \phi)) + \widetilde{B}_l(t) \sin(l(\theta_s + \phi)) \right] \right) d\theta_s. \end{aligned}$$

By expanding $\cos(l(\theta_s + \phi))$ and $\sin(l(\theta_s + \phi))$, and making use of the orthogonality of $\cos k\theta_s$ and $\sin k\theta_s$, we obtain

$$(22) \quad \rho_d(\phi) = \frac{1}{2\pi} + \pi \sum_{k=1}^{N-1} \left(\widetilde{A}_k^2(t) + \widetilde{B}_k^2(t) \right) \cos(k\phi).$$

From this formulation of the phase difference distribution in terms of the Fourier coefficients of the desired phase distribution, one can easily verify that $\rho_d(\phi)$ is 2π -periodic, $\int_0^{2\pi} \rho_d(\phi) d\phi = 1$, and $\rho_d(\phi)$ is independent of time, which can be seen by taking the time derivative of equation (22):

$$\begin{aligned} \dot{\rho}_d(\phi) &= \pi \sum_{k=1}^{N-1} 2 \left(\widetilde{A}_k(t) \dot{\widetilde{A}}_k(t) + \widetilde{B}_k(t) \dot{\widetilde{B}}_k(t) \right) \cos(k\phi) \\ &= \pi \sum_{k=1}^{N-1} 2k\omega \left(-\widetilde{A}_k(t) \widetilde{B}_k(t) + \widetilde{A}_k(t) \widetilde{B}_k(t) \right) \cos(k\phi) \\ &= 0 \end{aligned}$$

Another property that the phase difference distribution has is that it always has a local maximum at zero phase difference. This can easily be verified from equation (22), as $\frac{d\rho_d(0)}{d\phi} = 0$ and $\frac{d^2\rho_d(0)}{d\phi^2} < 0$.

3.2. Control Design. If for all k , $A_k(\tau) = \widetilde{A}_k(\tau)$ and $B_k(\tau) = \widetilde{B}_k(\tau)$, the phase distribution ρ would be equal to the desired distribution ρ_f at time τ . This motivates us to take our Lyapunov function as the sum of the squared differences of the Fourier coefficients of the current and the desired distribution:

$$(23) \quad V(t) = \frac{1}{2} \sum_{k=1}^{N-1} \left[\left(A_k(t) - \widetilde{A}_k(t) \right)^2 + \left(B_k(t) - \widetilde{B}_k(t) \right)^2 \right].$$

Thus the Lyapunov function is positive, and is zero only when $\rho(\theta, t) = \rho_f(\theta, t)$. Its derivative in time evolves as

$$(24) \quad \dot{V}(t) = I(t)u(t),$$

where $I(t)$ is given by the sum

$$(25) \quad I(t) = \sum_{k=1}^{N-1} \left[\left(B_k(t) - \widetilde{B}_k(t) \right) \mathcal{I}_{kB}(t) - \left(A_k(t) - \widetilde{A}_k(t) \right) \mathcal{I}_{kA}(t) \right].$$

Then by taking the control input $u(t) = -PI(t)$, where P is a positive scalar, we get the time derivative of the Lyapunov function, $\dot{V}(t) = -PI(t)^2$ as a negative scalar. Thus, according to the Lyapunov theorem, the control law $u(t) = -PI(t)$ will decrease the Lyapunov function until the current probability distribution becomes equal to the desired distribution. Here we do not consider the degenerate systems where $I(t) \equiv 0$ when $\rho(\theta, t) \neq \rho_f(\theta, t)$ (see Section 3.3 for such a system).

For both experimental and numerical reasons, it is more practical to have a bounded control input, so we take a ‘‘clipped’’ proportional control law

$$(26) \quad u(t) = \max(\min(u_{max}, -PI(t)), u_{min}).$$

Here u_{max} and u_{min} are the upper and lower bounds of the control input, respectively. The \max , and \min operators find the maximum and minimum of two scalars, respectively.

3.3. Degenerate Set. Note that for certain systems where $\rho(\theta, t) \neq \rho_f(\theta, t)$, equation (25) gives $I(t) \equiv 0$ for all time t , and the probability distribution $\rho(\theta, t)$ would not converge to the desired distribution $\rho_f(\theta, t)$. Here we derive the set of such phase distributions and PRCs that leads to this degeneracy, and give an example of such a system.

We can re-write $I(t)$ as

$$(27) \quad \begin{aligned} I(t) &= \frac{1}{\pi} \int_0^{2\pi} \sum_{k=1}^{N-1} k \left[\left(B_k(t) - \widetilde{B}_k(t) \right) \cos(k\theta) - \left(A_k(t) - \widetilde{A}_k(t) \right) \sin(k\theta) \right] \mathcal{Z}(\theta) \rho(\theta, t) d\theta \\ &= \frac{1}{\pi} \int_0^{2\pi} \left(\frac{\partial \rho}{\partial \theta} - \frac{\partial \rho_f}{\partial \theta} \right) \mathcal{Z}(\theta) \rho(\theta, t) d\theta. \end{aligned}$$

Now expanding $\rho(\theta, t)$, $\rho_f(\theta, t)$, and $\mathcal{Z}(\theta)$ into their complex Fourier series,

$$\begin{aligned}\rho(\theta, t) &= \sum_{k=1-N}^{N-1} a_k(t) \exp(ik\theta), & \rho_f(\theta, t) &= \sum_{k=1-N}^{N-1} \tilde{a}_k(t) \exp(ik\theta), \\ \mathcal{Z}(\theta) &= \sum_{k=1-N}^{N-1} c_k \exp(ik\theta),\end{aligned}$$

where

$$\begin{aligned}a_{\pm k}(t) &= \frac{A_k(t) \mp iB_k(t)}{2}, & \tilde{a}_{\pm k}(t) &= \frac{\tilde{A}_k(t) \mp i\tilde{B}_k(t)}{2}, \\ c_{\pm k} &= \frac{C_k \mp iS_k}{2}, & k &= 1, \dots, N-1, \\ a_0(t) &= A_0(t), & \tilde{a}_0(t) &= \tilde{A}_0(t), & c_0(t) &= C_0(t),\end{aligned}$$

we can write $I(t)$ from equation (27) as

$$(28) \quad I(t) = \sum_{p=1-N}^{N-1} \sum_{q=1-N}^{N-1} \sum_{r=1-N}^{N-1} \left[ip(a_p(t) - \tilde{a}_p(t)) c_q a_r(t) \frac{1}{\pi} \int_0^{2\pi} \exp(i(p+q+r)\theta) d\theta \right].$$

Thus the degenerate set of phase distributions and PRCs can be written in terms of their respective Fourier coefficients as

$$(29) \quad \sum_{p \in M} \sum_{q=1-N}^{N-1} \sum_{r=1-N}^{N-1} [i2p(a_p(t) - \tilde{a}_p(t)) c_q a_r(t) \delta_{p+q+r,0}] \equiv 0$$

for all time t , where M is the subset of integers ranging from $1-N$ to $N-1$ for which $a_p(t) \neq \tilde{a}_p(t)$, and $\delta_{p+q+r,0}$ is the Kronecker delta, which is equal to $1 \forall p+q+r=0$, and is 0 otherwise.

3.3.1. Degenerate System Example. As an example degenerate system, we consider the Type I PRC near a SNIPER bifurcation given by [8]

$$\mathcal{Z}(\theta) = \frac{2}{\omega} (1 - \cos(\theta)).$$

Thus $c_0 = 2/\omega$, $c_{\pm 1} = 1/\omega$, while rest of the PRC Fourier coefficients are 0. We take the desired distribution as a uniform distribution,

$$\rho_f(\theta, t) = \frac{1}{2\pi}.$$

Thus $\tilde{a}_0(t) = 1/2\pi$, while rest of the Fourier coefficients for ρ_f are 0 for all times. For the degenerate set, $I \equiv 0$, and thus $\rho(\theta, t)$ is a traveling wave moving in the $+\theta$ direction. We take it as

$$\rho(\theta, t) = \frac{\sin^2(\theta - \omega t)}{\pi}.$$

It is a physically realistic distribution since $\rho(\theta, t) \geq 0$, and $\int_0^{2\pi} \rho(\theta, t) d\theta = 1$. Thus $a_0(t) = 1/2\pi$, $a_{\pm 2}(t) = -\exp(\mp i2\omega t)/4\pi$, while rest of its Fourier coefficients are 0.

There are only two nonzero cases to consider in the summation of the degenerate set (equation (29)):

$$\begin{aligned} p = 2, q = 0, r = -2; \quad & i2(2) \left(-\frac{\exp(-i2\omega t)}{4\pi} - 0 \right) \left(\frac{2}{\omega} \right) \left(-\frac{\exp(i2\omega t)}{4\pi} \right) = \frac{i}{2\omega\pi^2}, \\ p = -2, q = 0, r = 2; \quad & -i2(2) \left(-\frac{\exp(i2\omega t)}{4\pi} - 0 \right) \left(\frac{2}{\omega} \right) \left(-\frac{\exp(-i2\omega t)}{4\pi} \right) = -\frac{i}{2\omega\pi^2}, \\ & I(t) = \frac{i}{2\omega\pi^2} - \frac{i}{2\omega\pi^2} = 0. \end{aligned}$$

Thus as I is zero even though the phase distributions are not equal, this is a degenerate system. This can also be verified by analytically evaluating the integral in equation (27) to be zero, i.e.,

$$\begin{aligned} I(t) &= \frac{4}{\omega\pi^3} \int_0^{2\pi} \sin^3(\theta - \omega t) \cos(\theta - \omega t) (1 - \cos \theta) d\theta \\ &= \frac{4}{\omega\pi^3} \left[\frac{\cos(\theta - 2\omega t) - \cos(2\theta - 2\omega t)}{8} + \frac{\cos(3\theta - 2\omega t)}{24} - \frac{\cos(3\theta - 4\omega t)}{48} \right. \\ &\quad \left. + \frac{\cos(4\theta - 4\omega t)}{32} - \frac{\cos(5\theta - 4\omega t)}{80} + \frac{3}{32} \right] \Big|_0^{2\pi} = 0. \end{aligned}$$

Note that such degeneracy arises due to the inherent simplicity and symmetry present in the system under consideration, and thus should not be considered a limitation of the devised control law. ‘‘Real world’’ systems would have more than two Fourier modes and some sort of asymmetry, which would avoid degeneracy.

3.4. Numerical Methods. Here we give details on the numerical methods we use for the simulation results that we present in the next section. Since we are dealing with periodic probability distributions in θ , we take the initial (and, later, the desired distributions) as a von Mises distribution [5]

$$(30) \quad \rho(\theta, 0) = \frac{e^{\kappa \cos(\theta + \theta_0)}}{2\pi \mathcal{I}_0(\kappa)},$$

with $\mathcal{I}_0(\kappa)$ the modified Bessel function of first kind of order 0. For such a distribution, the mean is θ_0 , and the variance is $1 - \mathcal{I}_1(\kappa)/\mathcal{I}_0(\kappa)$, where $\mathcal{I}_1(\kappa)$ is the modified Bessel function of first kind of order 1. The variance decreases as κ increases, and so the distribution becomes narrower and taller. To demonstrate the effectiveness of our control algorithm, we apply the control input given by equation (26) to a population of 100 phase oscillators

$$(31) \quad \dot{\Theta}_i(t) = \omega + \mathcal{Z}(\Theta_i(t))u(t), \quad i = 1, 2, \dots, 100.$$

For the case where initial distribution $\rho(\theta, 0)$ is a uniform distribution ($\kappa = 0$), we take the initial value of phase oscillators $\Theta_i(0) = 2\pi(i - 1)/100$, and for a non-zero κ , we use the

command `randraw('vonmises', [Theta_0, kappa], 100)` from the Circular Statistical toolbox developed for Matlab in [4] to initialize the phase oscillators corresponding to a von Mises distribution (equation (30)).

We discretize θ into a uniform mesh with $2N = 128$ grid points. We choose this grid size for a good spatial resolution of the probability distribution, and efficient computation of the fast Fourier transform algorithm. For computing the PRCs of the various models presented in next section, we use the XPP package [12] with a time step T/N . We scale the PRC computed by this package by ω , as we consider PRC as $\mathcal{Z}(\theta) = \frac{\partial \theta}{\partial \mathbf{x}}$, whereas the computed PRC from the XPP package is $\tilde{\mathcal{Z}}(t) = \frac{\partial t}{\partial \mathbf{x}}$ [8, 43]. Then we use the Matlab command `fft` to compute the Fourier coefficients of the initial distribution $\rho(\theta, 0)$. Note that the `fft` command computes coefficients of the complex Fourier series given as

$$\rho(\theta, 0) = \sum_{k=1-N}^N a_k(0) \exp(ik\theta),$$

giving an output $[a_0, a_1(0), \dots, a_N(0), a_{1-N}(0), a_{2-N}(0), \dots, a_{-1}(0)] \times 2N$. From these coefficients, we then compute the coefficients of the real Fourier series

$$\rho(\theta, 0) = A_0 + \sum_{k=1}^{N-1} A_k(0) \cos(k\theta) + B_k(0) \sin(k\theta),$$

as

$$\begin{aligned} A_0 &= a_0, \\ A_k(0) &= (a_k(0) + a_{-k}(0)), \\ B_k(0) &= i(a_k(0) - a_{-k}(0)). \end{aligned}$$

The same procedure is adopted to compute real Fourier coefficients of $\rho_f(\theta, 0)$ ($\tilde{A}_k(0)$, $\tilde{B}_k(0)$) and the PRC (C_k , S_k).

To evolve these coefficients over time, ODEs given by equations (16), (17), (20), (21) are evolved in time using a fourth order Runge-Kutta method with a fixed time step $dt = T/(8N)$. In order to maintain spectral accuracy, the integrals given by equations (18)-(19) are evaluated in Fourier space, i.e., we take the FFT of the integrand using Matlab command `fft`, and divide the first term of FFT by N to get the numerical value of the integral at every time step.

4. Applications. In this section, we apply the control law devised in the previous section to manipulate the population density of uncoupled noise free oscillators to achieve control objectives in a diversity of applications. These applications are desynchronizing an initially synchronized neuron population for the treatment of parkinsonian and essential tremor, forming neuron clusters from an initial desynchronized neuron population to maximize neural plasticity, and eliminating cardiac alternans by phase shifting a synchronized population of cardiac pacemaker cells. For all these applications, we consider underactuated dynamical systems with only one degree of actuation: the control input vector is $U(t) = [u(t), 0, \dots, 0]^T$. We make this assumption because in most conductance-based models of neurons and cardiac pacemaker cells, we can only give a single control input in the form of a current to one of the elements of the state vector, which corresponds to the voltage across the cell membrane.

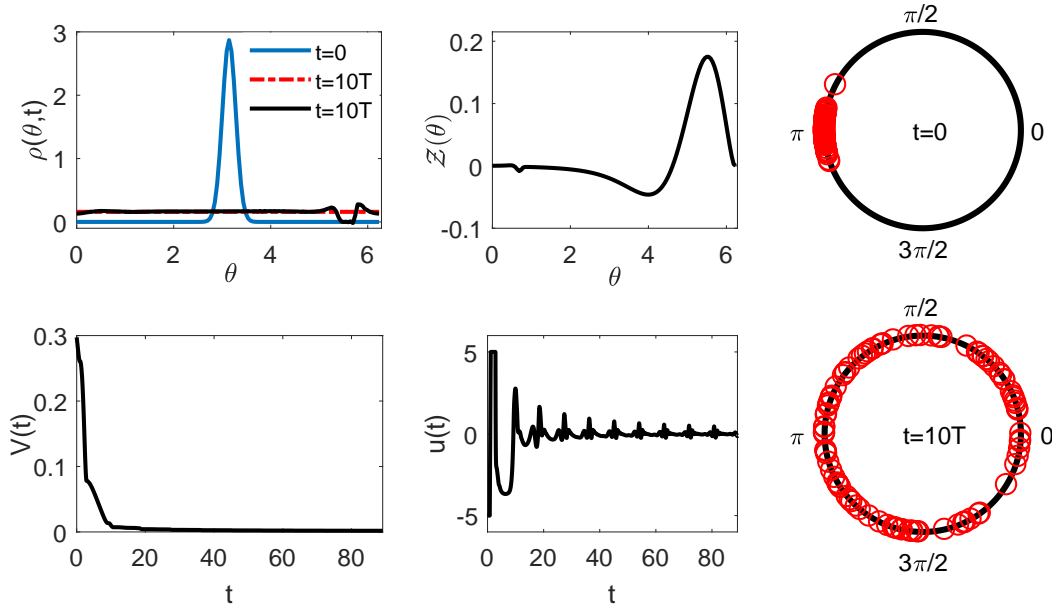


Figure 2. *Desynchronizing Control:* In the top left panel, the solid (resp., red dashed) lines show the probability distribution $\rho(\theta, t)$ (resp., $\rho_f(\theta, t)$) at various times. The top middle panel shows the PRC, while the bottom left and middle panels show the Lyapunov function $V(t)$ (23), and the control input, respectively. The top (resp., bottom) right panels show 100 phase oscillators at time $t = 0$ ms (resp., $t = 10T$ ms). Here $T = 8.91$ ms.

4.1. Desynchronizing Neurons. Parkinsonian and essential tremor affect millions of people worldwide, causing involuntary tremors in various parts of the body, and disrupting the activities of daily living. Pathological neural synchronization in the STN and the thalamus brain region is hypothesized to be one of the causes of motor symptoms of parkinsonian and essential tremor, respectively [28, 24]. Deep brain stimulation (DBS), an FDA approved treatment, has proven to alleviate these symptoms [2, 3] by stimulating the STN or the thalamus brain regions with a high frequency, (relatively) high energy pulsatile waveform, which has been hypothesized to desynchronize the synchronized neurons; see, e.g., [61, 63]. This has motivated researchers to come up with efficient model dependent control techniques [59, 44, 62] which not only desynchronize the neurons but also consume less energy, thus prolonging the battery life of the stimulator and preventing tissue damage or side effects caused by the pulsatile stimuli.

Thus, inspired by this treatment of parkinsonian and essential tremor, we employ our algorithm to desynchronize an initially synchronized population of neurons. Here we use our algorithm to change the probability distribution of synchronized neurons with mean π and $\kappa = 52$, into a uniform distribution ($\kappa = 0$). As a proof of concept, we use the two-dimensional reduced Hodgkin-Huxley model [25, 22] for calculating the PRC. For details of this model, see A.1. Under zero control input, this model gives a stable periodic orbit with time period $T = 8.91$ ms. The top middle panel of Figure 2 shows the corresponding PRC. We take the control parameters $P = 1000$, $u_{min} = -5$, $u_{max} = 5$, and simulate until $t = 10T$. From the

top and bottom left panels of Figure 2, we see that the control input is able to flatten out the bell shaped probability distribution, and thus decrease the Lyapunov function towards zero. For $t > 10 \text{ ms}$, we see that decay rate of Lyapunov function decreases, and thus the Lyapunov function asymptotically decreases towards zero. This can be explained from the equations (24 - 26) where we see that control input (decay rate of Lyapunov function) depends on the (square of) difference between current coefficients and desired coefficients. Thus as the coefficients get closer to their desired value, the magnitude of the control input decreases significantly, which decreases the rate of decay of the Lyapunov function. The top right panel of Figure 2 shows 100 phase oscillators synchronized with mean π , and $\kappa = 52$ extracted through the Matlab circular statistical toolbox. We apply the control input from the middle bottom panel of Figure 2 to them in an open loop manner. The bottom right panel of the same figure shows the same oscillators at time $t = 10T$. We see that the control input is able to desynchronize these oscillators almost perfectly. In transforming the probability distribution, the total control energy consumed comes out to be 141.78 units.

4.2. Clustering Neurons for Maximizing Neural Plasticity. An adult human brain is composed of hundreds of billions of neurons, and each of these neurons is connected to other neurons. Neural plasticity is a significant factor in forming specific connections by wiring neurons that fire together [53]. Spike time dependent plasticity (STDP) is one type of long-term plasticity, which wires neurons that fire together over a long period of time, thus helping in the regulation of neural synchrony. However, increased neural synchrony is a hallmark of several neurological disorders as discussed in the previous section, and STDP can resynchronize a desynchronized neural population over time in the presence of noise [50]. Thus, desynchronizing control, as considered in the previous section, may not be the best long-term solution. Recent results [63] suggest another hypothesis that DBS works by forming neural clusters instead of complete desynchronization. Coordinated Reset, a method which promotes clustering, has shown to have long lasting effects even after the control stimulus is turned off [59, 1]. This further motivates clustering as an alternative desynchronizing strategy for the treatment of parkinsonian and essential tremor. This would not only reduce neural synchrony but also promote clustering over long periods of time by re-wiring of neuron connections through STDP. We demonstrate this by the following analysis.

Let's suppose that we start with a desynchronized population. The average rate of synaptic connection change between any two neurons in the population is given by [50]

$$(32) \quad \Delta c = \int_0^{2\pi} \rho_d(\phi) S(\phi) d\phi.$$

A uniform phase distribution (desynchronized population) would result in a uniform phase difference distribution, which would lead to a zero average synaptic change. On the other hand, if we promote neural clustering, STDP would potentiate intra-cluster synaptic connections and depress inter-cluster connections. This would thus potentially help in long-term stabilizability of clusters in the presence of noise. We demonstrate this by taking two clusters and calculating the average synaptic change (32) intra- and inter-cluster. Thus we take the desired phase distribution as a bi-modal distribution, which can be realized as a sum of two uni-modal von

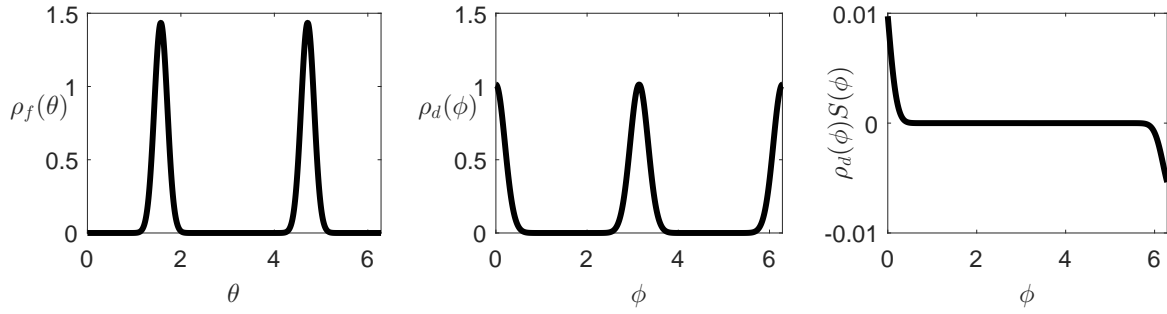


Figure 3. The left and the middle panel show the desired phase and phase difference distributions. The right panel shows the change in synaptic weight between two neurons as a function of their phase difference.

Mises distributions

$$(33) \quad \rho_f(\theta, t) = \frac{e^{\kappa \cos(\theta + \pi/2)} + e^{\kappa \cos(\theta + 3\pi/2)}}{4\pi\mathcal{I}_0(\kappa)},$$

where $\kappa = 52$. From this we calculate the phase difference distribution from equation (11) or (22), which can then be used to calculate the average synaptic change from equation (32). The left, middle, and right columns of Figure 3 show the desired phase distribution, phase difference distribution, and the product of the phase difference distribution with the STDP curve, (12) respectively. The average synaptic change for intra- and inter-cluster is calculated as

$$(34) \quad \Delta C_{intra-cluster} = \int_0^{\pi/2} \rho_d(\phi)S(\phi)d\phi + \int_{\frac{3\pi}{2}}^{2\pi} \rho_d(\phi)S(\phi)d\phi = 3.62 \times 10^{-4},$$

$$(35) \quad \Delta C_{inter-cluster} = \int_{\frac{\pi}{2}}^{\frac{3\pi}{2}} \rho_d(\phi)S(\phi)d\phi = -3.96 \times 10^{-7}.$$

Thus STDP would strengthen synapses in each cluster and weaken them between the two clusters, thereby potentially maintaining clusters over a long period of time. This motivates us to transform an initially desynchronized phase distribution ($\kappa = 0$) into a bi-modal phase distribution (33). As a proof of concept, here we again use the two-dimensional reduced Hodgkin-Huxley model for calculating the PRC. We take the control parameters $P = 1200$, $u_{min} = -15$, $u_{max} = 15$, and simulate until $t = 15T$. The results are shown in Figure 4. From the top and bottom left panels of Figure 4, we see that the control input is able to transform an initial uniform distribution into a bi-modal distribution, and thus the Lyapunov function decreases towards zero. As the Fourier coefficients of the current and desired distribution get closer, the control input decreases in magnitude, which decreases the rate of decay of the Lyapunov function. The top right panel of Figure 4 shows 100 desynchronized phase oscillators ($\Theta_i(0) = 2\pi(i-1)/100$) to which the control input from the middle bottom panel of Figure 4 is applied in an open loop manner. The bottom right panel of the same figure shows the oscillators at time $t = 15T$. We see that the control input is able to separate the desynchronized oscillators into two distinct clusters corresponding to the bi-modal

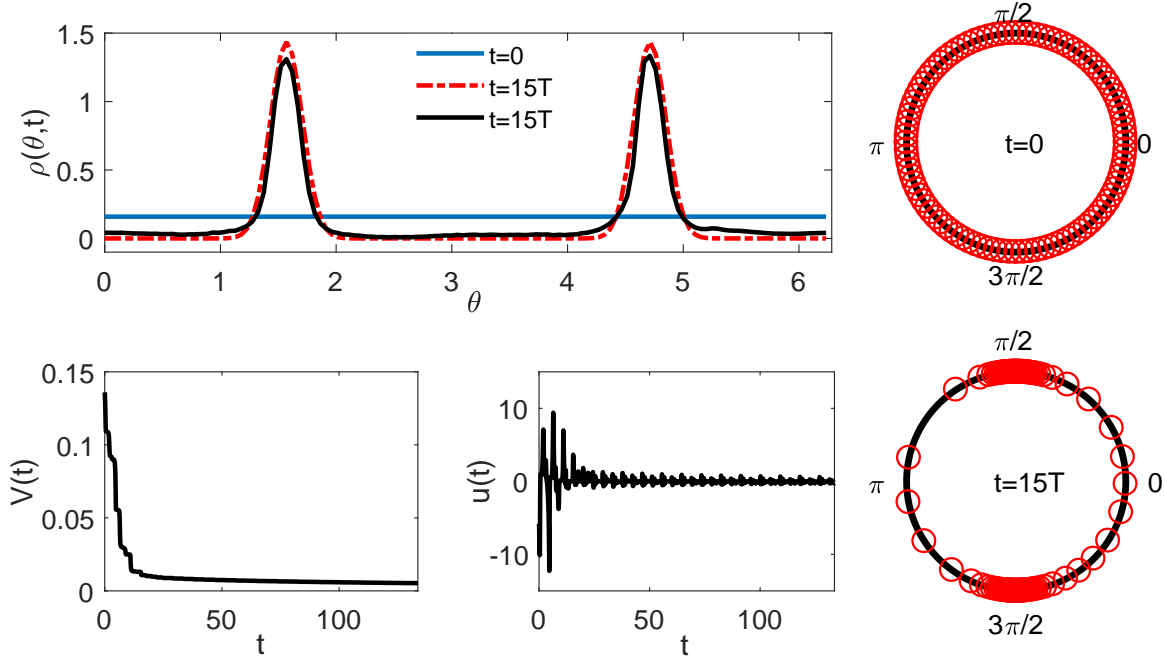


Figure 4. Clustering Control: In the top left panel, the solid (resp., red dashed) lines show the probability distribution $\rho(\theta, t)$ (resp., $\rho_f(\theta, t)$) at various times. The bottom left and middle panels show the Lyapunov function $V(t)$ (23), and the control input, respectively. The top (resp., bottom) right panels show 100 desynchronized (resp., clustered) phase oscillators at time $t = 0$ ms (resp., $t = 15T$ ms). Here $T = 8.91$ ms.

phase distribution distribution. In transforming the probability distribution, the total control energy consumed comes out to be 156.81 units.

4.3. Eliminating Cardiac Alternans. The collection of cells in the Sinoatrial node called cardiac pacemaker cells elicit periodic electrical pulses which polarize a collection of excitable and contractile cells called myocytes. In the process of depolarizing, myocytes contract and propagate action potentials to the neighboring cells. This well-coordinated process of excitation / depolarization and contraction enables the heart to pump blood throughout the body. Under normal conditions, with constant pacing by the cardiac pacemaker cells, the action potential duration (APD), that is the time for which an action potential lasts in a myocyte cell, also remains constant. However, under some conditions, this 1:1 rhythm between pacing and the APD can become unstable, bifurcating into a 2:2 rhythm of alternating long and short APD, known as alternans [36]. Alternans is observed to be a possible first step leading to fibrillation [47]. Thus, a number of researchers have worked on suppressing alternans as a method of preventing fibrillation, thereby preventing the need for painful and damaging defibrillating shocks. Many of these methods [19, 9, 20, 64] operate by exciting the myocardium tissue externally with periodic pulses, and changing the period according to the alternating rhythm. However, such a control requires excitation at several sites in the tissue [51].

In [41], we developed a novel strategy to suppress alternans by changing the phase of

the pacemaker cells. The control strategy was based on a single oscillator model to change the phase of a single cell. However for an effective cardiac alternans elimination, we need to consider the entire population of cardiac pacemaker cells which oscillate in synchrony. So, here we aim to phase shift the population of cardiac pacemaker cells using the control algorithm we developed in Section 3.2. Such a control strategy could eliminate the need to excite the tissue at multiple sites. The amount of phase change required to eliminate alternans depends on the discrete APD dynamics [41]. Here we advance the phase by $\pi/2$ as an example. For the PRC calculation, we consider phase reduction of the 7-dimensional YNI model of SA node cells in rabbit heart proposed in [68]. The model is of Hodgkin-Huxley type with 6 gating variables and a transmembrane voltage variable on which the control input acts. For details of the model, see A.2. With this model we get a stable periodic orbit with time period $T = 340.8$ ms. We start with a synchronous population distribution with mean $\pi/2$ and $\kappa = 52$. In order to phase shift this distribution by $\pi/2$, we take the target population distribution $\rho_f(\theta, t)$ with same κ value but an initial mean of π . Thus our control algorithm will push the distribution $\rho(\theta, t)$ forward until it matches with the desired distribution $\rho_f(\theta, t)$. We take the control parameters $P = 50$, $u_{min} = -5$, $u_{max} = 5$ and apply control input until $t = 5T$. From the top and bottom right panels of Figure 5, we see that the control input is able to phase shift the probability distribution, and thus decreases the Lyapunov function towards zero. In doing so, it changes the shape of the distribution slightly. The top right panel of Figure 5 shows 100 phase oscillators synchronized with mean $\pi/2$, and $\kappa = 52$ extracted through the Matlab circular statistical toolbox. We apply the control input from the middle bottom panel of the figure to them in an open loop manner. The bottom right panel of the same figure shows the oscillators at time $t = 5T$. We see that the control input is able to phase shift these oscillators by $\pi/2$. The slight change in shape of the phase distribution is reflected in the final position of phase oscillators, where handful of the oscillators get spread relative to the main cluster. In shifting the phase of the probability distribution, the total control energy consumed comes out to be 31.86 units.

Here we mention another application for which shifting the phase of an oscillator population is desired: phase shifting circadian oscillators for the treatment of jet lag. Neurons in the suprachiasmatic nucleus (SCN) of the brain are responsible for maintaining the circadian rhythm in mammals. This rhythm is synchronized with the external day and night cycle under normal conditions. A disruption between these two rhythms can happen due to multiple reasons, such as travel across time zones, starting a night shift job, working in extreme environments (space, earth poles, underwater), etc. Such asynchrony can lead to several physiological disorders [52, 26], thus motivating researchers to try to develop ways to remove it. In [41], we developed a strategy to eliminate this asynchrony by changing the phase of a single SCN neuron by using a light stimulus as the control input, since light is known to affect the circadian rhythm [10]. This would change the phase of the circadian rhythm so that it gets aligned with the external cycle after the end of the controlled oscillation. However for a better alignment of the circadian rhythm with the external environment, we need to phase shift the entire population of SCN neurons which oscillate in synchrony, which can be achieved by our control algorithm. This is very similar to the previous application of phase shifting cardiac pacemaker cells.

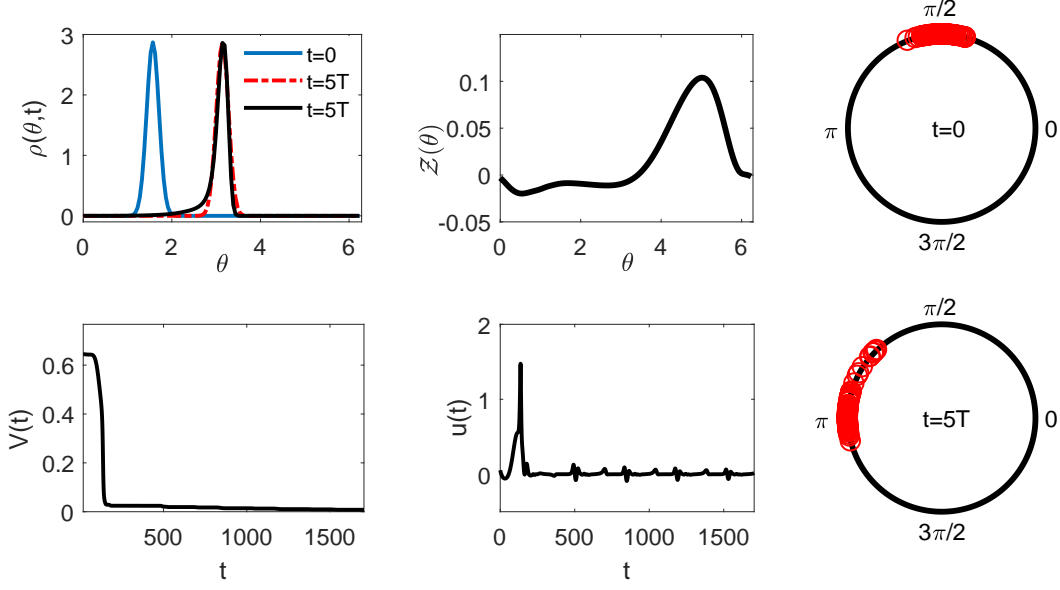


Figure 5. Phase shifting cardiac pacemaker cells: In the top left panel, the solid (resp., red dashed) lines show the probability distribution $\rho(\theta, t)$ (resp., $\rho_f(\theta, t)$) at various times. The top middle panel shows the PRC, while the bottom left and middle panels show the Lyapunov function $V(t)$ (23), and the control input respectively. The top (resp., bottom) right panels show 100 phase oscillators at time $t = 0$ ms (resp., $t = 5T$ ms). Here $T = 340.8$ ms. Note that in the absence of control input, the oscillators would have a mean of $\pi/2$ at $t = 5T$.

5. Addition of White Noise. So far we have demonstrated that our control is effective for a population of uncoupled, noise-free oscillators. However, real systems are subjected to noise. Thus in this section we modify our control to take this into account.

Given M noisy, uncoupled oscillators with dynamics given by

$$(36) \quad \frac{d\mathbf{x}_j}{dt} = F(\mathbf{x}_j) + \left[u(t) + \sqrt{2S}\eta_j(t), 0, \dots, 0 \right]^T, \quad j = 1, \dots, M.$$

Here each oscillator receives a common input $u(t)$ modified by a different realization of Gaussian white noise $\eta_j(t)$, with $\langle \eta_i(t)\eta_j(t') \rangle = \delta_{ij}\delta(t-t')$. Letting θ_j be the phase of the j^{th} oscillator, to leading order in the noise strength Ito's formula gives [16]

$$(37) \quad \dot{\theta}_j = \omega + \mathcal{Z}(\theta) \left[u(t) + \sqrt{2S}\eta_j(t) \right], \quad j = 1, \dots, M.$$

Assuming M is large and noise perturbations are small, the population dynamics can be represented in terms of its phase distribution $\rho(\theta, t)$ with stochastic averaging [14, 65]:

$$(38) \quad \frac{\partial \rho(\theta, t)}{\partial t} = -\frac{\partial}{\partial \theta} \left[(\omega + \mathcal{Z}(\theta)u(t)) \rho(\theta, t) \right] + \frac{B^2}{2} \frac{\partial^2 \rho(\theta, t)}{\partial \theta^2},$$

where

$$B^2 = \frac{2S}{2\pi} \int_0^{2\pi} \mathcal{Z}^2(\theta) d\theta.$$

As before, the desired final probability distribution $\rho_f(\theta, t)$ is taken to be a traveling wave which evolves according to equation (8). To devise our control laws, we use the approximation of a finite Fourier series to write the phase distributions (equations (13), and (14)). The Fourier coefficients of the desired phase distribution evolve as before (equations (20), and (21)), whereas the Fourier coefficients of phase distribution evolve as

$$(39) \quad \dot{A}_k(t) = -k\omega B_k - \mathcal{I}_{kA}(t)u(t) - \frac{B^2}{2}k^2 A_k(t),$$

$$(40) \quad \dot{B}_k(t) = k\omega A_k + \mathcal{I}_{kB}(t)u(t) - \frac{B^2}{2}k^2 B_k(t).$$

5.1. Control Design. Here as well we take the Lyapunov function as the sum of squared differences of the Fourier coefficients of the current and the desired distributions (equation (23)). Its derivative in time evolves as

$$(41) \quad \dot{V}(t) = I(t)u(t) + G(t),$$

where

$$G(t) = -\frac{B^2}{2} \sum_{k=1}^{N-1} k^2 \left[A_k(t) \left(A_k(t) - \widetilde{A}_k(t) \right) + B_k(t) \left(B_k(t) - \widetilde{B}_k(t) \right) \right].$$

Then by taking the control input

$$(42) \quad u(t) = -PI(t) - \frac{G(t)}{I(t)},$$

where P is a positive scalar, we get the time derivative of the Lyapunov function to be a negative scalar. Thus, according to the Lyapunov theorem, the control law (42) will decrease the Lyapunov function until the current probability distribution becomes equal to the desired distribution. Here we do not consider the degenerate case where $I(t) \equiv 0$ when $\rho(\theta, t) \neq \rho_f(\theta, t)$ (see Section 3.3 for cases when $I(t) \equiv 0$ when $\rho(\theta, t) \neq \rho_f(\theta, t)$).

5.2. Simulation Results. To demonstrate our control in the presence of noise, we use (42) to transform an initial uniform phase distribution into a desired bi-modal distribution (33). We take the noise strength $\sqrt{2S} = 0.05$ in equations (38) and (37). To simulate the noisy phase oscillators, we write the equation (37) as

$$d\theta_j = \omega dt + \mathcal{Z}(\theta) \left[u(t)dt + \sqrt{2S}dW_j(t) \right], \quad j = 1, \dots, M,$$

where $dW_j(t) = \eta_j(t)dt$ and $W_j(t)$ is the standard Wiener process. We use the second order Runge-Kutta algorithm developed in [23] to simulate the above equation, and use `randn` with a predefined seed in Matlab for generating the standard Wiener process. In order to be consistent, we evaluate the phase distribution and the control input using a second order Runge-Kutta method as well. As a proof of concept, here we again use the two-dimensional reduced Hodgkin-Huxley model for calculating the PRC. We take the control parameter $P =$

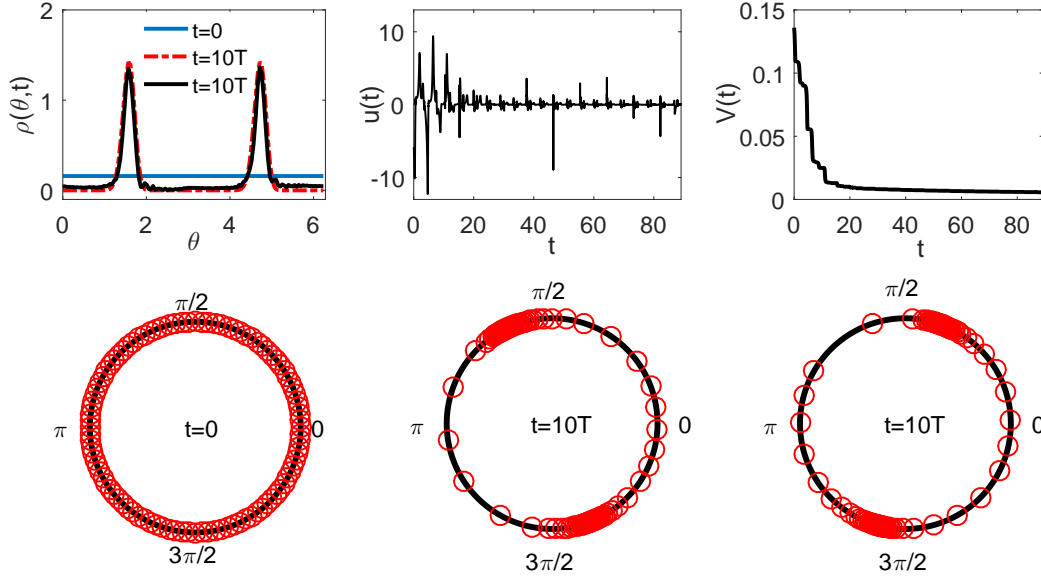


Figure 6. Clustering Control in presence of noise: In the top left panel, the solid (resp., red dashed) lines show the probability distribution $\rho(\theta, t)$ (resp., $\rho_f(\theta, t)$) at various times. The top middle and right panels show the control input (42), and the Lyapunov function $V(t)$ (23), respectively. The bottom left panel shows 100 desynchronized phase oscillators at time $t = 0$ ms. The bottom middle and right panels show the phase oscillators evaluated at time $t = 10$ ms according to (37) with the control input from top middle panel, but with different randn initial states. Here $T = 8.91$ ms.

1200, and simulate until $t = 10T$. The results are shown in Figure 6. From the top left and middle panels, we see that the control input is able to transform an initial uniform distribution into a bi-modal distribution, and thus the Lyapunov function decreases towards zero. The bottom left panel of Figure 6 shows 100 desynchronized phase oscillators to which the control input from the top middle panel of Figure 6 is applied in an open loop manner. We simulate these phase oscillators two times with different randn initial states. The bottom middle and right panels of Figure 6 show oscillators at time $t = 10T$ for these two simulations. The control input is able to separate the desynchronized oscillators into two distinct clusters corresponding to the bi-modal phase distribution distribution. However, noise makes the two clusters in the bottom middle and right panels of the figure drift by about 0.13π and 0.09π respectively. This is expected as white noise is known to change the period of an oscillator [39]. In transforming the probability distribution, the total control energy consumed comes out to be 158.18 units, which is 0.87% more than the similar control without noise. This is expected as the addition of white noise introduces a diffusion term in the phase distribution PDE, and thus causes the phase distribution to decay down towards a uniform distribution with time. So the control has to spend an additional effort in transforming the phase distribution into a bi-modal distribution.

6. Conclusion. In this article we developed a framework to control a population of uncoupled oscillators by controlling their phase distributions. By writing the phase distribution

as a finite Fourier series, we were able to decompose the PDE governing the evolution of the phase distribution into a set of ODEs governing the evolution of the corresponding Fourier coefficients. We formulated the control in Fourier space as well, driving the Fourier coefficients of the current phase distribution to the Fourier coefficients of the desired distribution with a single control input. We also constructed a degenerate set of phase distributions and the phase response curves in terms of their Fourier coefficients. Moreover, we showed that the control algorithm is quite flexible; for the systems considered in this paper, they have the potential to drive a system of uncoupled oscillators from any initial phase distribution to any traveling-wave final phase distribution, as long as the combination of those distributions is non-degenerate.

We demonstrated the versatility of our control algorithm by using it for three distinct applications. First, motivated by the hypothesis of neural synchronization in the STN and the thalamus brain region as one of the causes of motor symptoms of parkinsonian and essential tremor, respectively, we applied our control algorithm to drive an initial synchronous phase distribution to a uniform distribution. For the second application, we defined the phase difference distribution in terms of the phase distribution, and proved some of its fundamental properties. This formulation of the phase difference distribution was essential in demonstrating the importance of a clustered neural population for enhancing spike time dependent plasticity, and thus re-wiring of neural connections for better stability of the partially synchronous clustered state. Motivated by the elimination of cardiac alternans, we applied our algorithm to control a population of synchronized cardiac pacemaker cells by advancing their phase distribution by a specified phase. For all these applications, we demonstrated the effectiveness of our control by applying the respective control inputs to a population of 100 uncoupled noise-free phase oscillators. Finally, we devised a new control algorithm to take into account the effect of white noise on the dynamics of the oscillator population.

We conclude with remarks about the experimental implementation of these algorithms. Since they require knowledge of the current Fourier coefficients of the phase distribution, one would need to measure neuronal/cardiac pacemaker cell activity in order to back out the phase distribution and hence the Fourier coefficients in real time. This measurement would require good spatial and temporal resolution, so for both neuroscience and cardiovascular experiments we suggest that the use of Micro-Electrode arrays (MEA) would be a good fit. Note that for in vivo experiments, fMRI and EEG are unlikely to be the right tools since fMRI has poor temporal resolution, while EEG is susceptible to noise and poorly measures neural activity beneath the cortex. An experimental setup in general will include effects due to coupling, which are absent in our control algorithm. Our algorithm would still work on such systems as long as the coupling is weak. If synchrony is stable with coupling, then it would be harder for our control algorithm to desynchronize a synchronized population in the presence of coupling. The addition of noise might make this even harder if STDP is present, as STDP promotes synchrony in the presence of noise. However, in the absence of STDP, noise would make it easier for our control algorithm to desynchronize a synchronized oscillator population.

Appendix A. Models. In this appendix, we give details of the mathematical models used in this article.

A.1. Reduced Hodgkin-Huxley model. Here we list the reduced Hodgkin-Huxley model [38, 25, 22] used in Section 4.1:

$$\begin{aligned}\dot{v} &= (I - g_{Na}(m_\infty)^3(0.8 - n)(v - v_{Na}) - g_K n^4(v - v_K) - g_L(v - v_L)) / c + u(t), \\ \dot{n} &= a_n(1 - n) - b_n n,\end{aligned}$$

where v is the trans-membrane voltage, and n is the gating variable. I is the baseline current, for which we use the units $\mu A/cm^2$, and $u(t)$ represents the applied control current.

$$\begin{aligned}a_n &= 0.01(v + 55)/(1 - \exp(-(v + 55)/10)), \\ b_n &= 0.125 \exp(-(v + 65)/80), \\ a_m &= 0.1(v + 40)/(1 - \exp(-(v + 40)/10)), \\ b_m &= 4 \exp(-(v + 65)/18), \\ m_\infty &= a_m/(a_m + b_m), \\ c &= 1, \quad g_L = 0.3, \quad g_{Na} = 120, \quad v_{Na} = 50 \\ g_K &= 36, \quad v_K = -77, \quad v_L = -54.4 \quad I = 20.\end{aligned}$$

Here, $\theta = 0$ corresponds to the initial condition $v = 42.8828$, $n = 0.4920$.

A.2. YNI model. Here we list model parameters of the YNI model [68] introduced in Section 4.3. It is given as

$$\begin{aligned}\dot{v} &= -\frac{I_{Na} + I_k + I_l + I_s + I_h}{C} + u(t), \\ \dot{d} &= \alpha_d(1 - d) - \beta_d d, \\ \dot{f} &= \alpha_f(1 - f) - \beta_f f, \\ \dot{m} &= \alpha_m(1 - m) - \beta_m m, \\ \dot{h} &= \alpha_h(1 - h) - \beta_h h, \\ \dot{q} &= \alpha_q(1 - q) - \beta_q q, \\ \dot{p} &= \alpha_p(1 - p) - \beta_p p,\end{aligned}$$

where v represents the transmembrane voltage, and d, f, m, h, q, p are the gating variables, $u(t)$ represents the applied current as the control input, with parameters

$$\begin{aligned}\alpha_d &= \frac{0.01045(v + 35)}{(1 - \exp(-(v + 35)/2.5)) + \frac{0.03125v}{(1 - \exp(-v/4.8))}}, \\ \beta_d &= 0.00421(v - 5)/(-1 + \exp((v - 5)/2.5)), \\ \alpha_f &= 0.000355(v + 20)/(-1 + \exp((v + 20)/5.633)), \\ \beta_f &= 0.000944(v + 60)/(1 + \exp(-(v + 29.5)/4.16)), \\ \alpha_m &= (v + 37)/(1 - \exp(-(v + 37)/10)), \\ \beta_m &= 40 \exp(-0.056(v + 62)), \\ \alpha_h &= 0.001209(\exp(-(v + 20)/6.534)), \\ \beta_h &= 1/(1 + \exp(-(v + 30)/10)),\end{aligned}$$

$$\begin{aligned}
\alpha_q &= 0.0000495 + \frac{0.00034(v + 100)}{(-1 + \exp((v + 100)/4.4))}, \\
\beta_q &= 0.0000845 + 0.0005(v + 40)/(1 - \exp(-(v + 40)/6)), \\
\alpha_p &= 0.0006 + 0.009/(1 + \exp(-(v + 3.8)/9.71)), \\
\beta_p &= 0.000225(v + 40)/(-1 + \exp((v + 40)/13.3)), \\
i_s &= 12.5(\exp((v - 30)/15) - 1), \\
I_s &= (0.95d + 0.05)(0.95f + 0.05)i_s, \\
I_{Na} &= 0.5m^3h(v - 30), \\
I_h &= 0.4q(v + 25), \\
I_k &= 0.7p(\exp(0.0277(v + 90)) - 1)/\exp(0.0277(v + 40)), \\
I_l &= 0.8(-\exp(-(v + 60)/20) + 1), \\
C &= 1.
\end{aligned}$$

Here, $\theta = 0$ corresponds to the initial condition $v = -19.2803$, $d = 0.6817$, $f = 0.0236$, $m = 0.8540$, $h = 0.0013$, $q = 0.0038$, $p = 0.6592$.

section*ACKNOWLEDGMENT This work was supported by National Science Foundation Grant No. NSF-1635542. We thank Prof. Gary Froyland for helpful discussions during the initial stage of this project. We thank Timothy Matchen for pointing out the non-degeneracy issue, and Raphael Egan for helpful discussions on the pseudospectral method.

REFERENCES

- [1] I. ADAMCHIC, C. HAUPTMANN, U. BARNIKOL, N. PAWELCZYK, O. POPOVYCH, T. BARNIKOL, A. SILCHENKO, J. VOLKMANN, G. DEUSCHL, W. MEISSNER, M. MAAROUF, V. STURM, H. FREUND, AND P. TASS, *Coordinated reset neuromodulation for parkinson's disease: Proof-of-concept study*, *Movement Disorders*, 29 (2014), pp. 1679–1684, <https://doi.org/10.1002/mds.25923>, <https://onlinelibrary.wiley.com/doi/abs/10.1002/mds.25923>, <https://arxiv.org/abs/https://onlinelibrary.wiley.com/doi/pdf/10.1002/mds.25923>.
- [2] A. BENABID, S. CHABARDES, J. MITROFANIS, AND P. POLLAK, *Deep brain stimulation of the subthalamic nucleus for the treatment of Parkinson's disease*, *The Lancet Neurology*, 8 (2009), pp. 67–81, [https://doi.org/10.1016/S1474-4422\(08\)70291-6](https://doi.org/10.1016/S1474-4422(08)70291-6).
- [3] A. BENABID, P. POLLAK, D. HOFFMANN, C. GERVASON, M. HOMMEL, J. PERRET, J. DE ROUGEMONT, AND D. GAO, *Long-term suppression of tremor by chronic stimulation of the ventral intermediate thalamic nucleus*, *The Lancet*, 337 (1991), pp. 403–406, [https://doi.org/10.1016/0140-6736\(91\)91175-T](https://doi.org/10.1016/0140-6736(91)91175-T).
- [4] P. BERENS, *Circstat: A Matlab toolbox for circular statistics*, *Journal of Statistical Software*, Articles, 31 (2009), pp. 1–21, <https://doi.org/10.18637/jss.v031.i10>, <https://www.jstatsoft.org/v031/i10>.
- [5] D. BEST AND N. FISHER, *Efficient simulation of the von mises distribution*, *Journal of the Royal Statistical Society. Series C (Applied Statistics)*, 28 (1979), pp. 152–157, <http://www.jstor.org/stable/2346732>.
- [6] G. BI AND M. POO, *Synaptic modifications in cultured hippocampal neurons: Dependence on spike timing, synaptic strength, and postsynaptic cell type*, *Journal of Neuroscience*, 18 (1998), pp. 10464–10472, <http://www.jneurosci.org/content/18/24/10464>.
- [7] G. BI AND M. POO, *Synaptic modification by correlated activity: Hebb's postulate revisited*, *Annual Review of Neuroscience*, 24 (2001), pp. 139–166, <https://doi.org/10.1146/annurev.neuro.24.1.139>, <https://doi.org/10.1146/annurev.neuro.24.1.139>.
- [8] E. BROWN, J. MOEHLIS, AND P. HOLMES, *On the phase reduction and response dynamics of neural oscillator populations*, *Neural Comp.*, 16 (2004), pp. 673–715, <https://doi.org/10.1162/089976604322860668>.

- [9] D. CHRISTINI, M. RICCIO, C. CULIANU, J. FOX, A. KARMA, AND R. GILMOUR JR, *Control of electrical alternans in canine cardiac Purkinje fibers*, Physical Review Letters, 96 (2006), p. 104101, <https://doi.org/10.1103/PhysRevLett.96.104101>.
- [10] C. CZEISLER, R. KRONAUER, J. ALLAN, J. DUFFY, M. JEWETT, E. BROWN, AND J. RONDA, *Bright light induction of strong (type 0) resetting of the human circadian pacemaker*, Science, 2 (1989), p. 4, <https://doi.org/10.1126/science.2734611>.
- [11] P. DANZL AND J. MOEHLIS, *Event-based feedback control of nonlinear oscillators using phase response curves*, in Decision and Control, 2007 46th IEEE Conference on, IEEE, 2007, pp. 5806–5811, <https://doi.org/10.1109/CDC.2007.4434505>.
- [12] B. ERMENTROUT, *Simulating, Analyzing, and Animating Dynamical Systems: A Guide to XPPAUT for Researchers and Students*, vol. 14, SIAM, Philadelphia, 2002, <https://doi.org/10.1137/1.9780898718195>.
- [13] D. FORGER AND D. PAYDARFAR, *Starting, stopping, and resetting biological oscillators: in search of optimum perturbations*, Journal of Theoretical Biology, 230 (2004), pp. 521–532, <https://doi.org/10.1016/j.jtbi.2004.04.043>.
- [14] M. I. FREIDLIN AND A. D. WENTZELL, *Random Perturbations*, Springer New York, New York, NY, 1998, pp. 15–43, https://doi.org/10.1007/978-1-4612-0611-8_2, https://doi.org/10.1007/978-1-4612-0611-8_2.
- [15] R. FRIEDRICH AND M. STOPFER, *Recent dynamics in olfactory population coding*, Current Opinion in Neurobiology, 11 (2001), pp. 468–474, [https://doi.org/10.1016/S0959-4388\(00\)00236-1](https://doi.org/10.1016/S0959-4388(00)00236-1).
- [16] C. GARDINER, P. ZOLLER, AND P. ZOLLER, *Quantum Noise: A Handbook of Markovian and Non-Markovian Quantum Stochastic Methods with Applications to Quantum Optics*, Springer Series in Synergetics, Springer, 2004, <https://www.springer.com/us/book/9783540223016>.
- [17] C. GRAY, P. KÖNIG, A. ENGEL, AND W. SINGER, *Oscillatory responses in cat visual cortex exhibit inter-columnar synchronization which reflects global stimulus properties*, Nature, 338 (1989), pp. 334–337, <https://doi.org/10.1038/338334a0>.
- [18] J. GUCKENHEIMER, *Isochrons and phaseless sets*, Journal of Mathematical Biology, 1 (1975), pp. 259–273, <https://doi.org/10.1007/BF01273747>.
- [19] G. HALL AND D. GAUTHIER, *Experimental control of cardiac muscle alternans*, Physical Review Letters, 88 (2002), p. 198102, <https://doi.org/10.1103/PhysRevLett.88.198102>.
- [20] K. HALL, D. CHRISTINI, M. TREMBLAY, J. COLLINS, L. GLASS, AND J. BILLETTE, *Dynamic control of cardiac alternans*, Physical Review Letters, 78 (1997), p. 4518, <https://doi.org/10.1103/PhysRevLett.78.4518>.
- [21] D. HEBB, *The Organization of Behavior*, Wiley: New York, 1949.
- [22] A. L. HODGKIN AND A. F. HUXLEY, *A quantitative description of membrane current and its application to conduction and excitation in nerve*, The Journal of Physiology, 117 (1952), pp. 500–544, <https://doi.org/10.1113/jphysiol.1952.sp004764>, <http://dx.doi.org/10.1113/jphysiol.1952.sp004764>.
- [23] R. HONEYCUTT, *Stochastic runge-kutta algorithms. i. white noise*, Phys. Rev. A, 45 (1992), pp. 600–603, <https://doi.org/10.1103/PhysRevA.45.600>, <https://link.aps.org/doi/10.1103/PhysRevA.45.600>.
- [24] A. KANE, W. HUTCHISON, M. HODAIE, A. LOZANO, AND J. DOSTROVSKY, *Enhanced synchronization of thalamic theta band local field potentials in patients with essential tremor*, Experimental Neurology, 217 (2009), pp. 171–176, <https://doi.org/10.1016/j.expneurol.2009.02.005>.
- [25] J. KEENER AND J. SNEYD, *Mathematical Physiology*, Springer-Verlag New York, Inc., New York, NY, USA, 1998, https://doi.org/10.1007/978-0-387-75847-3_1.
- [26] E. KLERMAN, *Clinical aspects of human circadian rhythms*, Journal of Biological Rhythms, 20 (2005), pp. 375–386, <https://doi.org/10.1177/0748730405278353>.
- [27] W. KLIMESCH, *Memory processes, brain oscillations and EEG synchronization*, International Journal of Psychophysiology, 24 (1996), pp. 61–100, [https://doi.org/10.1016/S0167-8760\(96\)00057-8](https://doi.org/10.1016/S0167-8760(96)00057-8).
- [28] A. KÜHN, A. TSUI, T. AZIZ, N. RAY, C. BRÜCKE, A. KUPSCH, G.-H. SCHNEIDER, AND P. BROWN, *Pathological synchronisation in the subthalamic nucleus of patients with Parkinson's disease relates to both bradykinesia and rigidity*, Experimental Neurology, 215 (2009), pp. 380–387, <https://doi.org/10.1016/j.expneurol.2008.11.008>.
- [29] Y. KURAMOTO, *Chemical Oscillations, Waves, and Turbulence*, Springer, Berlin, 1984.
- [30] Y. KURAMOTO, *Phase-and center-manifold reductions for large populations of coupled oscillators with*

- application to non-locally coupled systems*, International Journal of Bifurcation and Chaos, 7 (1997), pp. 789–805, <https://doi.org/10.1142/S0218127497000595>.
- [31] K. KURITZ, W. HALTER, AND F. ALLGÖWER, *Passivity-Based Ensemble Control for Cell Cycle Synchronization*, Springer International Publishing, Emerging Applications of Control and Systems Theory, 2018, pp. 1–13, https://doi.org/10.1007/978-3-319-67068-3_1, https://doi.org/10.1007/978-3-319-67068-3_1.
- [32] H. MARKRAM, W. GERSTNER, AND P. SJSTRM, *Spike-Timing-Dependent Plasticity: A Comprehensive Overview*, Frontiers Research Foundation, 2012, <https://doi.org/10.3389/fnsyn.2012.00002>.
- [33] T. MATCHEN AND J. MOEHLIS, *Real-time stabilization of neurons into clusters*, in 2017 American Control Conference (ACC), May 2017, pp. 2805–2810, <https://doi.org/10.23919/ACC.2017.7963376>.
- [34] T. MATCHEN AND J. MOEHLIS, *Phase model-based neuron stabilization into arbitrary clusters*, Journal of Computational Neuroscience, 44 (2018), pp. 363–378, <https://doi.org/10.1007/s10827-018-0683-y>, <https://doi.org/10.1007/s10827-018-0683-y>.
- [35] D. C. MICHAELS, E. P. MATYAS, AND J. JALIFE, *Mechanisms of sinoatrial pacemaker synchronization: a new hypothesis.*, Circulation Research, 61 (1987), pp. 704–714, <https://doi.org/10.1161/01.RES.61.5.704>, <http://circres.ahajournals.org/content/61/5/704>, <https://arxiv.org/abs/http://circres.ahajournals.org/content/61/5/704.full.pdf>.
- [36] G. MINES, *On dynamic equilibrium in the heart*, The Journal of Physiology, 46 (1913), pp. 349–383, <https://doi.org/10.1113/jphysiol.1913.sp001596>.
- [37] D. MINORS, J. WATERHOUSE, AND A. WIRZ-JUSTICE, *A human phase-response curve to light*, Neuroscience Letters, 133 (1991), pp. 36–40, [https://doi.org/10.1016/0304-3940\(91\)90051-T](https://doi.org/10.1016/0304-3940(91)90051-T).
- [38] J. MOEHLIS, *Canards for a reduction of the hodgkin-huxley equations*, Journal of Mathematical Biology, 52 (2006), pp. 141–153, <https://doi.org/10.1007/s00285-005-0347-1>, <https://doi.org/10.1007/s00285-005-0347-1>.
- [39] J. MOEHLIS, *Improving the precision of noisy oscillators*, Physica D: Nonlinear Phenomena, 272 (2014), pp. 8–17, <https://doi.org/10.1016/j.physd.2014.01.001>.
- [40] J. MOEHLIS, E. SHEA-BROWN, AND H. RABITZ, *Optimal inputs for phase models of spiking neurons*, Journal of Computational and Nonlinear Dynamics, 1 (2006), pp. 358–367, <https://doi.org/10.1115/1.2338654>.
- [41] B. MONGA AND J. MOEHLIS, *Optimal phase control of biological oscillators using augmented phase reduction*, Biological Cybernetics, (2018), <https://doi.org/10.1007/s00422-018-0764-z>, <https://doi.org/10.1007/s00422-018-0764-z>.
- [42] B. MONGA AND J. MOEHLIS, *Synchronizing and desynchronizing neural populations through phase distribution control*, in 2018 American Control Conference (ACC), June 2018, pp. 2808–2813.
- [43] B. MONGA, D. WILSON, T. MATCHEN, AND J. MOEHLIS, *Phase reduction and phase-based optimal control for biological systems: A tutorial*, Under Review, (2018).
- [44] A. NABI, M. MIRZADEH, F. GIBOU, AND J. MOEHLIS, *Minimum energy desynchronizing control for coupled neurons*, Journal of Computational Neuroscience, 34 (2013), pp. 259–271, <https://doi.org/10.1007/s10827-012-0419-3>.
- [45] A. NABI AND J. MOEHLIS, *Nonlinear hybrid control of phase models for coupled oscillators*, in American Control Conference (ACC), 2010, IEEE, 2010, pp. 922–923, <https://doi.org/10.1109/ACC.2010.5530681>.
- [46] A. NABI, T. STIGEN, J. MOEHLIS, AND T. NETOFF, *Minimum energy control for in vitro neurons*, Journal of Neural Engineering, 10 (2013), p. 036005, <https://doi.org/10.1088/1741-2560/10/4/049501>.
- [47] J. PASTORE, S. GIROUARD, K. LAURITA, F. AKAR, AND D. ROSENBAUM, *Mechanism linking T-wave alternans to the genesis of cardiac fibrillation*, Circulation, 99 (1999), pp. 1385–1394, <https://doi.org/10.1161/01.CIR.99.10.1385>.
- [48] C. S. PESKIN, *Mathematical aspects of heart physiology*, Courant Institute of Mathematical Sciences, (1975), pp. 268–278, <https://www.math.nyu.edu/faculty/peskin/heartnotes/index.html>.
- [49] A. PIKOVSKY, M. ROSENBLUM, AND J. KURTHS, *Synchronization: A Universal Concept in Nonlinear Sciences*, University Press, 2003, <https://books.google.com/books?id=B1hQlwEACAAJ>.
- [50] O. POPOVYCH, S. YANCHUK, AND P. TASS, *Self-organized noise resistance of oscillatory neural networks with spike timing-dependent plasticity*, Scientific Reports, 3, <https://doi.org/http://dx.doi.org/10.1038/srep02926>.

- [51] W.-J. RAPPEL, F. FENTON, AND A. KARMA, *Spatiotemporal control of wave instabilities in cardiac tissue*, Physical Review Letters, 83 (1999), p. 456, <https://doi.org/10.1103/PhysRevLett.83.456>.
- [52] M. REA, A. BIERMAN, M. FIGUEIRO, AND J. BULLOUGH, *A new approach to understanding the impact of circadian disruption on human health*, Journal of Circadian Rhythms, 6 (2008), p. 7, <https://doi.org/10.1186/1740-3391-6-7>.
- [53] C. SHATZ, *The developing brain*, Scientific American, 267 (1992), pp. 60–67, <http://www.jstor.org/stable/24939213>.
- [54] A. SHERMAN AND J. RINZEL, *Model for synchronization of pancreatic beta-cells by gap junction coupling*, Biophysical Journal, 59 (1991), pp. 547 – 559, [https://doi.org/10.1016/S0006-3495\(91\)82271-8](https://doi.org/10.1016/S0006-3495(91)82271-8), <http://www.sciencedirect.com/science/article/pii/S0006349591822718>.
- [55] R. SNARI, M. TINSLEY, D. WILSON, S. FARAMARZI, T. NETOFF, J. MOEHLIS, AND K. SHOWALTER, *Desynchronization of stochastically synchronized chemical oscillators*, Chaos: An Interdisciplinary Journal of Nonlinear Science, 25 (2015), p. 123116, <https://doi.org/10.1063/1.4937724>.
- [56] G. STENT, *A physiological mechanism for Hebb’s postulate of learning*, Proceedings of the National Academy of Sciences, 70 (1973), pp. 997–1001.
- [57] T. STIGEN, P. DANZL, J. MOEHLIS, AND T. NETOFF, *Controlling spike timing and synchrony in oscillatory neurons*, Journal of Neurophysiology, 105 (2011), p. 2074, <https://doi.org/10.1186/1471-2202-12-S1-P223>.
- [58] P. TASS, *Effective desynchronization by means of double-pulse phase resetting*, EPL (Europhysics Letters), 53 (2001), p. 15, <https://doi.org/10.1209/epl/i2001-00117-6>.
- [59] P. TASS, *A model of desynchronizing deep brain stimulation with a demand-controlled coordinated reset of neural subpopulations*, Biological Cybernetics, 89 (2003), pp. 81–88, <https://doi.org/10.1007/s00422-003-0425-7>.
- [60] P. TASS, *Phase Resetting in Medicine and Biology: Stochastic Modelling and Data Analysis*, Springer-Verlag Berlin Heidelberg, 2007, <https://doi.org/10.1007/978-3-540-38161-7>.
- [61] C. WILSON, B. BEVERLIN, AND T. NETOFF, *Chaotic desynchronization as the therapeutic mechanism of deep brain stimulation*, Front. Syst. Neurosci., 5 (2011), <https://doi.org/10.3389/fnsys.2011.00050>.
- [62] D. WILSON AND J. MOEHLIS, *Optimal chaotic desynchronization for neural populations*, SIAM Journal on Applied Dynamical Systems, 13 (2014), p. 276, <https://doi.org/10.1137/120901702>.
- [63] D. WILSON AND J. MOEHLIS, *Clustered desynchronization from high-frequency deep brain stimulation*, PLoS Comput. Biol., 11 (2015), p. e1004673, <https://doi.org/10.1371/journal.pcbi.1004673>.
- [64] D. WILSON AND J. MOEHLIS, *Extending phase reduction to excitable media: theory and applications*, SIAM Review, 57 (2015), pp. 201–222, <https://doi.org/10.1137/140952478>.
- [65] D. WILSON AND J. MOEHLIS, *Isostable reduction with applications to time-dependent partial differential equations*, Physical Review E, 94 (2016), p. 012211, <https://doi.org/10.1103/PhysRevE.94.012211>, <https://link.aps.org/doi/10.1103/PhysRevE.94.012211>.
- [66] A. WINFREE, *Biological rhythms and the behavior of populations of coupled oscillators*, Journal of Theoretical Biology, 16 (1967), pp. 15–42, [https://doi.org/10.1016/0022-5193\(67\)90051-3](https://doi.org/10.1016/0022-5193(67)90051-3).
- [67] A. WINFREE, *The Geometry of Biological Time, Second Edition*, Springer, New York, 2001, <https://doi.org/10.1007/978-1-4757-3484-3>.
- [68] K. YANAGIHARA, A. NOMA, AND H. IRISAWA, *Reconstruction of sino-atrial node pacemaker potential based on the voltage clamp experiments.*, The Japanese Journal of Physiology, 30 (1980), pp. 841–857, <https://doi.org/10.2170/jjphysiol.30.841>.
- [69] J. ZHANG, J. WEN, AND A. JULIUS, *Optimal circadian rhythm control with light input for rapid entrainment and improved vigilance*, in Proceedings of the 51st IEEE Conference on Decision and Control (CDC), IEEE, 2012, pp. 3007–3012, <https://doi.org/10.1109/CDC.2012.6426226>.
- [70] L. I. ZHANG, H. TAO, C. HOLT, W. HARRIS, AND M. POO, *A critical window for cooperation and competition among developing retinotectal synapses*, Nature, 395, <https://doi.org/10.1038/25665>, <http://dx.doi.org/10.1038/25665>.
- [71] A. ZLOTNIK, Y. CHEN, I. KISS, H. TANAKA, AND J.-S. LI, *Optimal waveform for fast entrainment of weakly forced nonlinear oscillators*, Physical Review Letters, 111 (2013), p. 024102, <https://doi.org/10.1103/PhysRevLett.111.024102>.

This figure "Fig4.png" is available in "png" format from:

<http://arxiv.org/ps/1811.10562v1>

This figure "alternans.png" is available in "png" format from:

<http://arxiv.org/ps/1811.10562v1>